Available online at www.sciencedirect.com
SCIENCE DIRECT
Journal of Catalysis 241 (2006) 14–19
JOURNAL OF CATALYSIS
www.elsevier.com/locate/jcat

Growth and structural stability of well-ordered PdZn alloy nanoparticles

Simon Penner [a,*], Bernd Jenewein [a], Harald Gabasch [a,b], Bernhard Klötzer [a], Di Wang [b], Axel Knop-Gericke [b], Robert Schlögl [b], Konrad Hayek [a]

[a] *Institute of Physical Chemistry, University of Innsbruck, Innrain 52a, A-6020 Innsbruck, Austria*
[b] *Department of Inorganic Chemistry, Fritz-Haber-Institut of the Max-Planck Society, Faradayweg 4-6, D-14195 Berlin, Germany*

Received 16 February 2006; revised 3 April 2006; accepted 6 April 2006

Available online 15 May 2006

Abstract

Despite many recent attempts to unravel the structure of novel PdZn alloys, which are promising catalysts in methanol steam reforming, a detailed study on the formation of Pd–Zn alloy particles and of their structural and thermal stability is still missing. We take advantage of the unique properties of epitaxially grown Pd particles embedded in layers of amorphous ZnO and mechanically stabilized by SiO_2, and present an electron microscopy study of the preparation of well-ordered PdZn alloy nanoparticles at surprisingly low reduction temperatures. These are formed by topotactic growth on the surface of the Pd nanoparticles and are structurally and thermally stable in a broad temperature range (473–873 K). At and above 873 K, partial decomposition of PdZn and the start of interaction with the SiO_2 support are observed.

Keywords: Thin film model catalyst; Hydrogen reduction; Alloy formation; Electron microscopy; Selected area electron diffraction

1. Introduction

Much recent effort has been invested in the development of suitable catalysts for methanol steam reforming [1–15], which is one of the most promising processes for hydrogen production, with a high hydrogen/carbon ratio [16]. Cu/ZnO catalysts have been used commercially to produce hydrogen with high selectivity and activity [2–6], but they suffer from deactivation at reaction temperatures above 573 K [17]. Recently, novel Pd/ZnO systems [3–15] (as well as Pd/Ga_2O_3 and Pd/In_2O_3 [18,19]) have attracted increased attention because of their enhanced long-term and thermal stability [20,21]. Because unsupported pure Pd exhibits only poor selectivity [22], the observed high activity and selectivity for CO_2 formation was ascribed to the formation of distinct PdZn, PdIn, and PdGa alloys on reductive activation at elevated temperatures [18]. The best characterized of these is the Pd/ZnO system, in which alloy formation has been studied and confirmed by X-ray diffraction (XRD) [18,23], temperature-programmed reduction (TPR) [18,23], X-ray spectroscopy (XPS), and ultraviolet photoelectron spectroscopy (UPS) [24–26]. Iwasa et al. [23] observed PdZn alloy formation on reduction at very low temperatures ($\geqslant$473 K). Density functional studies have revealed a close relationship between the electronic structure of PdZn- and Cu-based catalysts, giving rise to similar catalytic performance in methanol steam reforming [27,28]. Comparatively few studies on the structural characterization of the PdZn alloys by electron microscopy have been carried out, and these have been limited to overview imaging of powder catalysts in the as-prepared state and after hydrogen reduction, thereby mainly supporting XRD measurements [29,30]. The Pd–Zn system is known to form several stable bulk alloy phases [31], the most important and thermally most stable of which is the PdZn ($\beta 1$) phase, which crystallizes in a tetragonal (AuCu-type) $L1_0$ structure [32]. A key aspect to understand the catalytic peculiarities of the above-mentioned Pd–Zn alloy particles is determining their surface composition. Recent experiments in our laboratory [33] showed that a well-ordered $[(4/3 \times \sqrt{3}) \times 6]$ Pd–Zn layer forms on Pd(111) under UHV conditions at elevated temperatures.

Despite the importance of PdZn alloys for hydrogen production by steam reforming, detailed transmission electron microscopy (TEM) studies of their morphology and structure are

* Corresponding author. Fax: +43 512 507 2925.
E-mail address: simon.penner@uibk.ac.at (S. Penner).

0021-9517/$ – see front matter
doi:10.1016/j.jcat.2006.04.005

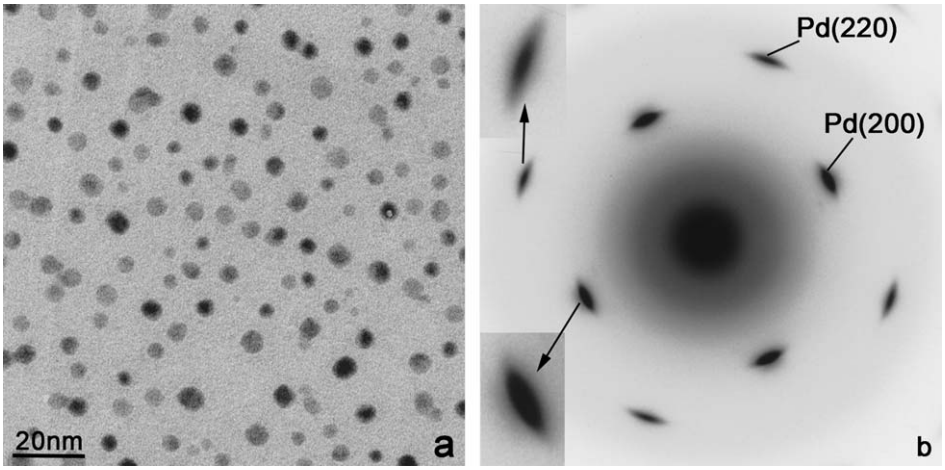

Fig. 1. (a) TEM overview of as-deposited Pd particles and ZnO/SiO_2 support, (b) corresponding SAED pattern.

not yet available. Consequently, the aim of the present study is to exploit the capabilities of modern electron microscopes in resolving the atomic structure of catalysts and to start from well-defined Pd particles, epitaxially grown on NaCl(001) cleavage faces and subsequently embedded in a layer of ZnO, to prepare distinct PdZn alloys. We present the first high-resolution images of well-defined PdZn alloy particles and propose a mechanism of their formation, as well as detailed information on their thermal and structural stability.

2. Experimental

Pd metal was deposited by electron-beam evaporation onto a freshly cleaved NaCl(001) plane at a base pressure of 10^{-4} Pa and a substrate temperature of 623 K. Under these experimental conditions, the deposition of Pd films of about 0.5 nm nominal thickness results in well-shaped Pd particles about 5 nm in size. Subsequently, the Pd particles were covered by a layer of amorphous ZnO at a template temperature of 523 K and mechanically stabilized by a supporting layer of amorphous SiO_2 (nominal thickness: 25 nm), deposited at room temperature. The ZnO was prepared by resistive heating of Zn metal in 10^{-2} Pa O_2, and the SiO_2 thin film was prepared by resistive heating of SiO in 10^{-2} Pa O_2. NaCl was subsequently removed by dissolution in distilled water; after careful rinsing, the resulting thin films were dried and mounted on gold grids for electron microscopy. Reductive treatments (1 bar H_2 for 1 h) were performed in parallel in a flow system and a circulating batch reactor between 473 and 873 K. Structural and morphological changes were followed by high-resolution TEM (HRTEM), selected area electron diffraction (SAED), and energy-dispersive X-ray spectroscopy (EDXS). The electron micrographs were taken with a Zeiss EM 10C and a Philips CM FEG 200 microscope equipped with a Gatan image filter GIF100. The SAED patterns were calibrated with respect to the Pd spots in the as-grown state of the catalyst.

3. Results and discussion

The TEM overview in Fig. 1a shows the as-deposited state of the Pd catalyst, to which we reference all structural alterations occurring on reductive activation. The Pd particles are visible as dark and gray dots with a mean diameter of ∼5 nm. A particle density of around 6.8×10^7 particles/cm^2 was estimated by evaluating a number of TEM images from different parts of the sample. The dark particles are perfectly aligned along the Bragg orientation; the gray ones are tilted slightly out of the respective Bragg position. Most of the particles exhibit square or rectangular shapes, whereas some have more rounded outlines. Weak-beam dark field images of the corresponding alumina-based Pd thin film catalysts reveal the cuboctahedral habit of these particles [34]. Their almost perfect relative orientation with respect to the former NaCl(001) single crystal substrate is confirmed by the SAED pattern (Fig. 1b), exhibiting only reflections of the fcc structure of the Pd particles oriented along the [001] zone axis, that is, Pd(200) and Pd(220) spots (enlarged insets show symmetrical Pd reflections). No reflections arising from other orientations are present. The HRTEM images of cuboctahedral particles (Fig. 2) show mainly (200) lattice fringes of fcc Pd [d_{200}(Pd) = 0.1945 nm], including a 45-degree angle with the (111) cuboctaeder faces [34]. Hence, most Pd particles exhibit (001) base planes perpendicular to the electron beam. Both the ZnO and the SiO_2 supports are amorphous in the as-grown state. The amount of deposited ZnO was verified by EDXS to be close to the amount of deposited Pd.

No significant changes in particle structure or morphology are noted on reduction at temperatures below 473 K (1 bar hydrogen for 1 h). However, considerable alterations in both morphology and composition are introduced when the reduction temperature is raised to 523 K (Fig. 3). The particle size is increased slightly compared with the as-deposited state (mean diameter: 5.3 nm; particle density: 5.6×10^7 particles/cm^2), and recrystallization has occurred. A major part (about 80–90%) of the particles now show either randomly arranged sharp edges (denoted "A" in Fig. 3a) or square and rectangular outlines (denoted as "B" in Fig. 3a). This morphology is in striking contrast to both the as-grown state of this catalyst (10–20%

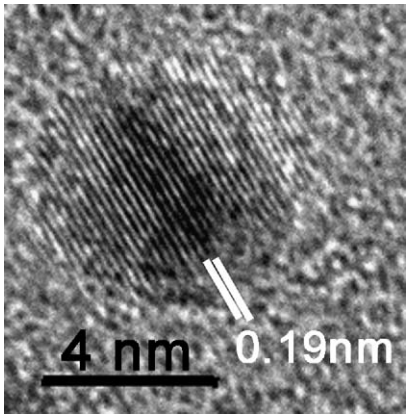

Fig. 2. HRTEM image of an as-grown Pd particle exhibiting (200) lattice fringes.

sharp-edged particles; Fig. 1a) and the state of a Pd/SiO_2 reference catalyst without ZnO, but treated under otherwise identical conditions (1 bar H_2 for 1 h at 523 K; see Figs. 3c and d), as discussed below. The SAED patterns of Fig. 3b show a "doubling" of both the Pd (200) and the Pd (220) spots (see enlarged insets), especially in comparison with Fig. 1b; that is, new reflections arise at $d \approx 0.144$ nm and $d \approx 0.205$ nm, and four new spot reflections appear at $d \approx 0.291$ nm, rotated by 45 degrees with respect to the Pd (200) spots. These new reflections perfectly match the (112), (200), and (110) reflections of the tetragonal PdZn alloy phase [($L1_0$ AuCu-type structure) [32] (d_{112}(PdZn) = 0.1449 nm, d_{200}(PdZn) = 0.205 nm, d_{110}(PdZn) = 0.290 nm)], which was formed to some extent during reductive activation even at 473 K. We emphasize that this newly formed alloy phase grows in almost perfect crystallographic relationship to the underlying Pd lattice (Pd [100]//PdZn [011]). The PdZn alloy formation is further corroborated by parallel high-resolution imaging. Fig. 4 shows a single PdZn alloy particle along with its fast Fourier transform (FFT). According to the FFT, the lattice fringes can be attributed to the (100) and (0–11) distances of the tetragonal PdZn crystal structure [32]. Hence the particle is oriented along its [011] zone axis. Similar effects have already been observed on the corresponding Pt/SiO_2 [35] and Pt/CeO_2 [36] systems. On the Pd/SiO_2 reference catalyst without ZnO, which exhibits an identical as-grown state and was reduced under otherwise identical conditions, the introduction of higher-indexed facets, manifested as a rounding of particles in TEM [34] and a considerable increase in particle size due to coalescence was observed (Fig. 3c), in strong contrast to the effects observed on $Pd/ZnO/SiO_2$ (Fig. 3a). Compared with the $Pd/ZnO/SiO_2$ catalyst, the SAED patterns of Pd/SiO_2 catalysts after reduction

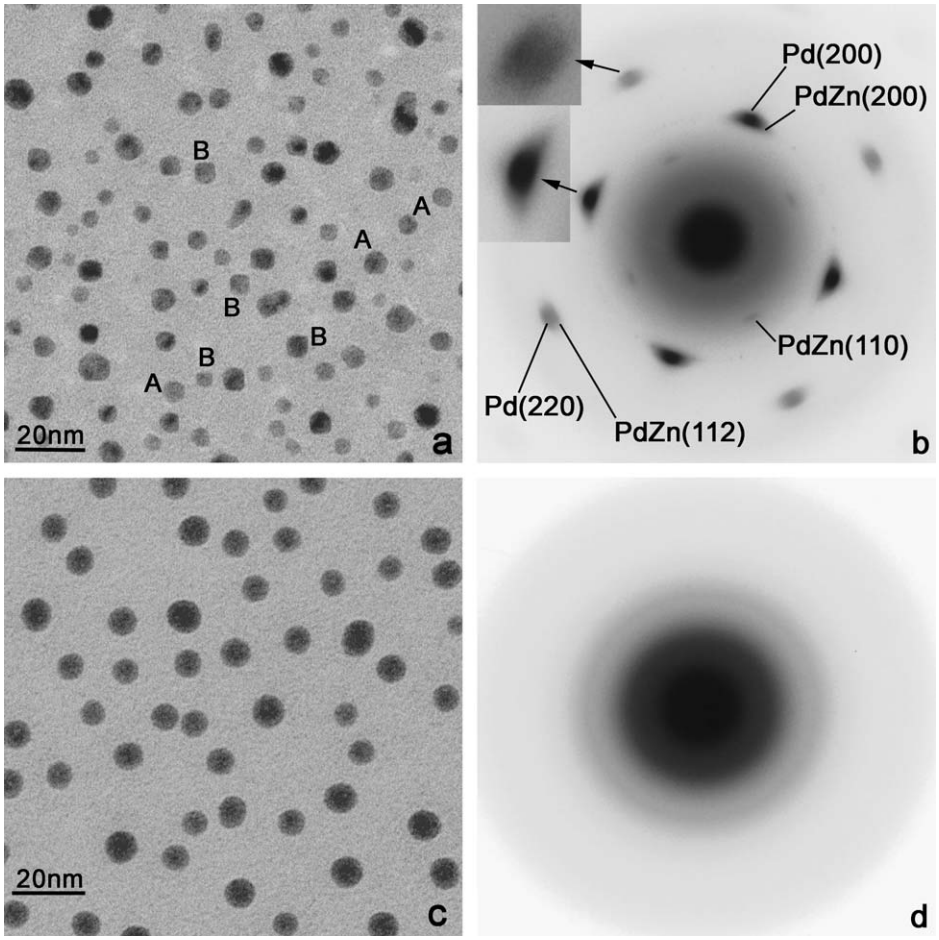

Fig. 3. (a) TEM overview of the $Pd/ZnO/SiO_2$ catalyst after reduction in 1 bar hydrogen at 523 K for 1 h, (b) corresponding SAED pattern; (c) TEM overview of the Pd/SiO_2 reference catalyst after reduction in 1 bar hydrogen at 523 K for 1 h, (d) corresponding SAED pattern.

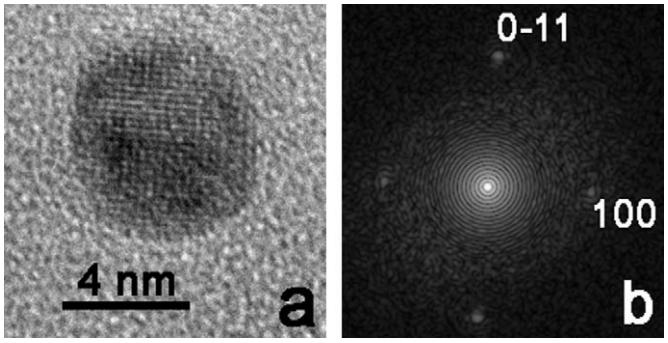

Fig. 4. (a) HRTEM image of a single-crystalline PdZn particle on its [011] zone axis, (b) corresponding FFT from the single particle area selected by a round mask. By doing so, only the contrast of the particle contributes to the FFT, though some nodal rings can be produced around the center of the FFT.

at 523 K (Fig. 3d) clearly reflect a trend toward amorphous structures, which may be interpreted in terms of Pd hydride formation [37]. From the comparison of Figs. 3a and b on the one hand and Figs. 3c and d on the other hand, it is obvious that the aforementioned recrystallization of the Pd particles in contact with ZnO must be closely associated with the process of alloy formation. Thus, adding ZnO to the Pd/SiO_2 system structurally stabilizes the Pd particles by Pd–Zn alloy formation compared with Pd/SiO_2, and also prevents the formation of an amorphous hydride phase. Furthermore, this protection against hydride formation by the presence of ZnO infers that the particles are covered by a shell of well-ordered PdZn alloy already at low reduction temperatures. This growth mechanism is confirmed by the fact that at and below 523 K, metallic Pd is still present with no indication of hydride formation, as well as by the perfect epitaxial relationship between Pd and PdZn. Most likely, a metastable PdZn alloy skin is formed *before* alloying proceeds into deeper regions of the Pd particles. Fig. 4 shows a HR image of a single PdZn alloy particle in the state of complete transformation already after reduction at 523 K. Because the SAED pattern shows metallic Pd remaining on the catalyst, complete PdZn particles as shown in Fig. 4 are still the minority species after reduction at 523 K, the majority must consist of PdZn-encapsulated Pd particles, a conclusion necessitated by the missing hydride formation and the inherent instability of pure Pd metal to amorphization under identical experimental conditions.

This "partially alloyed" state of the catalyst is stable up to 523 K. After reduction above 600 K, the Pd reflections vanish, and only alloy-induced diffraction spots remain. TEM images obtained after reduction at 723 K (Fig. 5a) reveal that the particle size again has slightly increased (mean diameter: 5.5 nm; particle density: 5.2×10^7 particles/cm^2), confirming the high thermal stability of the PdZn alloy compared with the as-grown state and the state after reduction at 523 K. SAED patterns (Fig. 5b) show broadened PdZn reflections, indicating a slight azimuthal disorder of the alloy particles. However, because no higher-order reflections of the tetragonal alloy structure are visible, it is clear that no additional particle zone axes contribute to the diffraction pattern. This highlights the great structural stability of the completed Pd–Zn alloy particles.

By reduction at and above 873 K (Figs. 6a and b), again some structural alterations are observed. Most of the particles did not undergo coalescence, but appear thermally and structurally stable even at and above 873 K (denoted as "A" in Fig. 6a). Nevertheless, some considerably larger particles (denoted as "B" in Fig. 6a) are formed, obviously by consuming closely neighboring particles. It is noteworthy that the sharp-angled particles have almost completely vanished and that most particles now exhibit more rounded outlines. Increasing disorder is also evidenced by the SAED patterns in Fig. 6b. The PdZn (110) and (200) spots appear broadened and faint, pointing to an increasing loss of orientational order and/or partial decomposition of the PdZn alloy. In addition, the formation of a Pd_2Si alloy phase is documented by the SAED pattern (Fig. 6b) and by high-resolution imaging (inset in Fig. 6a), indicating that the stability limit of the $Pd/ZnO/SiO_2$ catalyst is reached at about 900 K. Weak Pd_2Si (111) and (210) reflections, the latter overlapping with the broadened PdZn(200) spots, appear in the electron diffraction patterns. The HRTEM image of a single Pd_2Si alloy particle (along with its FFT) as shown in the inset of Fig. 6a indicates that the particle is oriented along its [2–15] zone axis. Therefore, the state of the catalyst after reduction at 873 K can be characterized as a coexistence of PdZn and Pd_2Si alloy phases.

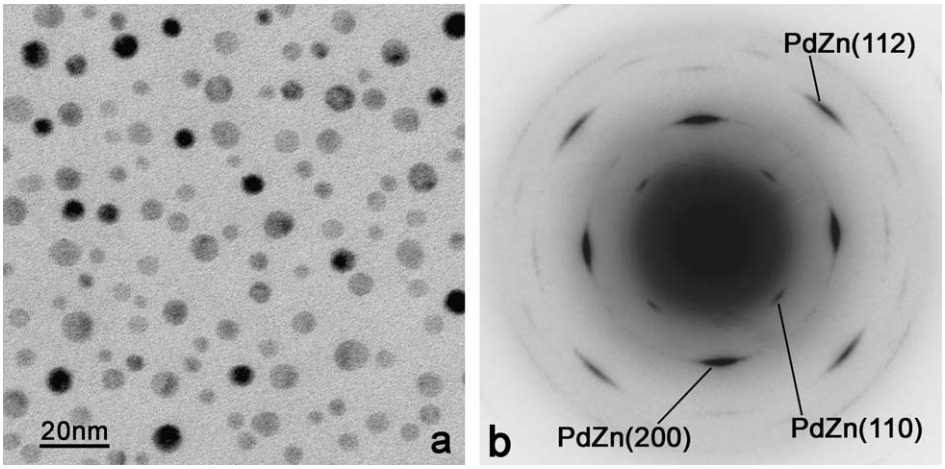

Fig. 5. (a) TEM overview of the $Pd/ZnO/SiO_2$ thin film catalyst after reduction in 1 bar hydrogen at 723 K for 1 h, (b) corresponding SAED pattern.

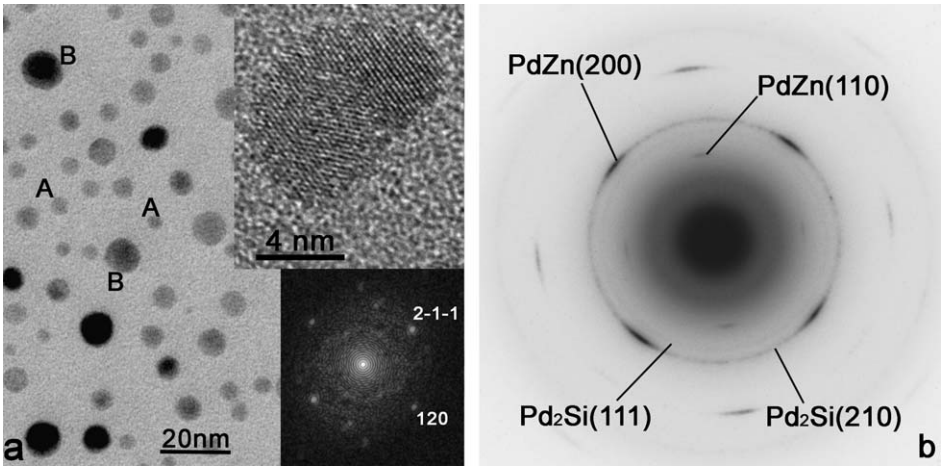

Fig. 6. State of the Pd/ZnO/SiO_2 catalyst after reduction in 1 bar H_2 at 873 K for 1 h. (a) TEM overview, (b) SAED pattern. Inset: HRTEM image of a [2,–1,5] oriented Pd_2Si particle with its FFT.

In line with previous studies on PdZn formation [8,12–14], the present electron microscopy study unambiguously reveals the onset of formation of a tetragonal PdZn phase upon reduction at or above 473 K. The formation of the alloy phase proceeds most likely via topotactic formation of PdZn on top of the Pd particles. This growth mechanism is likely favored by the relatively small mismatch of the lattice constants of fcc Pd (0.388 nm) and tetragonal PdZn (0.410 nm). We emphasize that the properties of the special thin film model catalysts used in the present study favor the alloying kinetics. Compared with conventional impregnated catalysts, the thin film systems are known for large and intimate contact between metal and support and defined particle size and shape (which makes them well suited for plan view lattice imaging by HRTEM).

4. Conclusion

The main conclusions of the present work can be summarized as follows. PdZn alloy particles are thermally and structurally stable on reduction between 473 and 873 K. Even above 873 K, only partial decomposition of the PdZn alloy is observed, accompanied by strong interaction with the SiO_2 support and resulting in the formation of Pd-rich silicides. This broad stability range is clearly due to the strong interaction of Pd with the ZnO support and the high stability of the 1:1 PdZn alloy phase. The strong particle stabilization effect (SPSE) is important for catalytic processes, such as methanol steam reforming and methanol synthesis on Pd/ZnO catalysts. In particular, the striking differences between the Pd/SiO_2 and Pd/ZnO/SiO_2 systems demonstrated in this work may lead to a better understanding of the drastic activity and selectivity differences between Pd/SiO_2 and Pd/ZnO reported in the literature [13,23]. According to recent single-crystal experiments [33,38] and theory studies [38,39] it seems that this PdZn alloy phase is stable over a wide temperature range.

Acknowledgment

H.G. thanks the Max Planck Society for a FHI research grant.

References

[1] H. Kobayashi, N. Takezawa, C. Minochi, J. Catal. 69 (1981) 487.
[2] T.-J. Huang, S.-W. Wang, Appl. Catal. 24 (1986) 287.
[3] T.-J. Huang, S.-L. Chren, Appl. Catal. 40 (1988) 43.
[4] S. Velu, K. Suzuki, M.P. Kapoor, F. Ohashi, T. Osaki, Appl. Catal. A 213 (2001) 47.
[5] S. Velu, K. Suzuki, M. Okazaki, M.P. Kapoor, T. Osaki, F. Ohashi, J. Catal. 194 (2000) 373.
[6] S. Murcia-Mascarós, R.M. Navarro, L. Gomez-Sainero, U. Costantino, M. Nocchetti, L.G. Fierro, J. Catal. 198 (2001) 338.
[7] N. Iwasa, S. Kudo, H. Takahashi, S. Masuda, N. Takezawa, Catal. Lett. 19 (1993) 211.
[8] N. Iwasa, S. Masuda, N. Takezawa, React. Kinet. Catal. Lett. 55 (1995) 349.
[9] M.L. Cubeiro, J.L.G. Fierro, J. Catal. 179 (1998) 150.
[10] M.L. Cubeiro, J.L.G. Fierro, Appl. Catal. A 168 (1998) 307.
[11] Y.-H. Chin, R. Dagle, J. Hu, A.C. Dohnalkova, Y. Wang, Catal. Today 77 (2002) 79.
[12] N. Iwasa, T. Mayanagi, S. Masuda, N. Takezawa, React. Kinet. Catal. Lett. 69 (2000) 355.
[13] N. Iwasa, T. Mayanagi, W. Nomura, M. Arai, N. Takezawa, Appl. Catal. A 248 (2003) 153.
[14] N. Iwasa, W. Nomura, T. Mayanagi, S. Fujita, M. Arai, N. Takezawa, J. Chem. Eng. Jpn. 37 (2004) 286.
[15] Y. Suwa, S.-I. Ito, S. Kameoka, K. Tomishige, K. Kunimori, Appl. Catal. A 267 (2004) 9.
[16] R. Peters, H.G. Dunsterwald, B. Hohlein, J. Power Sources 86 (2000) 507.
[17] D.L. Trimm, Z.I. Önsan, Catal. Rev. 43 (2001) 31.
[18] N. Iwasa, N. Takezawa, Top. Catal. 22 (3–4) (2003) 215.
[19] N. Iwasa, S. Masuda, N. Ogawa, N. Takezawa, Appl. Catal. A 125 (1995) 145.
[20] S. Liu, K. Takahashi, M. Ayabe, Catal. Today 87 (2003) 247.
[21] S. Liu, K. Takahashi, K. Uematsu, M. Ayabe, Appl. Catal. A 277 (2004) 265.
[22] N. Takezawa, N. Iwasa, Catal. Today 36 (1997) 45.
[23] N. Iwasa, T. Mayanagi, N. Ogawa, K. Sakata, N. Takezawa, Catal. Lett. 54 (1998) 119.

[24] A. Bayer, K. Flechtner, R. Denecke, H.-P. Steinrück, K.M. Neyman, N. Rösch, Surf. Sci. 600 (2006) 78.
[25] N. Iwasa, N. Ogawa, S. Masuda, N. Takezawa, Bull. Chem. Soc. Jpn. 71 (1998) 1451.
[26] S. Liu, K. Takahashi, K. Fuchigami, K. Uematsu, Appl. Catal. A 299 (2006) 58.
[27] Z.-X. Chen, K.M. Neyman, A.B. Gordienko, N. Rösch, Phys. Rev. B 68 (2003) 75417.
[28] Z.-X. Chen, K.M. Neyman, N. Rösch, Surf. Sci. 548 (2004) 291.
[29] J. Agrell, G. Germani, S.G. Järas, M. Boutonnet, Appl. Catal. A 242 (2003) 233.
[30] Y. Suwa, S. Ito, S. Kameoka, K. Tomishige, K. Kunimori, Appl. Catal. A 267 (2004) 9.
[31] Landolt, Börnstein, Phase Equilibria, Crystallographic and Thermodynamic Data of Binary Alloys, vol. 5, Springer, Berlin, 1998.
[32] H. Nowotny, H. Bitter, Monatsh. Chemie 81 (1950) 679.
[33] H. Gabasch, S. Penner, B. Jenewein, B. Klötzer, A. Knop-Gericke, D. Wang, R. Schlögl, K. Hayek, J. Phys. Chem. B, in press.
[34] G. Rupprechter, K. Hayek, L. Rendon, J.M. Yacaman, Thin Solid Films 260 (1995) 148.
[35] D. Wang, S. Penner, D.S. Su, G. Rupprechter, K. Hayek, R. Schlögl, J. Catal. 219 (2003) 434.
[36] S. Penner, D. Wang, R. Podloucky, R. Schlögl, K. Hayek, Phys. Chem. Chem. Phys. 6 (2004) 5244.
[37] S. Penner, B. Jenewein, H. Gabasch, B. Klötzer, D. Wang, A. Knop-Gericke, R. Schlögl, K. Hayek, J. Catal., in press.
[38] A. Bayer, K. Flechtner, R. Denecke, H.-P. Steinrück, K.N. Neyman, N. Rösch, Surf. Sci. 600 (2006) 78.
[39] Z. Chen, K.N. Neyman, N. Rösch, Surf. Sci. 548 (2004) 291.